JOURNAL OF PROPULSION AND POWER
Vol. 14, No. 2, March–April 1998

Laser Propulsion System for Space Vehicles

Aviad Brandstein*
Israeli Air Force, Israel
and
Yeshayahou Levy†
Technion–Israel Institute of Technology, Technion City, Haifa 32000, Israel

Propulsion of a space vehicle by means of a laser beam is among several innovative propulsion concepts currently being studied. The main advantage gained is the low-weight system, from decoupling the energy source from the space vehicle, and the low fuel consumption, thus achieving high levels of thrust and specific impulse. This paper concerns the design of a laser propulsion system based on the repetitively pulsed method, while taking into consideration the relevant physical processes occurring inside the engine, namely, inverse bremsstrahlung and the laser detonation wave. A feasibility study was conducted for a Hohmann orbital transfer, using an engine with a parabolic nozzle that focuses a projected laser beam to its focal region, enabling gas ionization and plasma ignition. The focusing of the laser beam was studied according to the ray-tracing technique. Mathematical simulation was applied to investigate the effect of the nozzle wall roughness to determine the sensitivity of laser intensity distribution within the focal region (and hence the size of the preliminary ionized volume) to nozzle surface quality. Results show that for elevating a satellite weighing 500 kg from 300 to 36,000 km above Earth, a suitable engine can be designed, producing 19,600 N with I_{sp} of 1200 s. A laser power of 400 MW is required to perform the maneuver, with 10,000 pulses per second of 30-ns duration at an energy level of about 50 kJ per pulse.

Nomenclature

A_i = roughness amplitude, $i = 1–4$
D = laser beam diameter at the transmitter
D^* = cold gas flow valve diameter
E = laser pulse energy
e = gas energy per unit mass
$\bar{F}$ = average thrust
f = laser pulse frequency
g = Earth gravity acceleration
h = gas enthalpy preunit mass
I = laser intensity
I_{sp} = specific impulse
I_0 = nominal laser intensity along the nozzle symmetry line
K = absorption coefficient
k = roughness length scale
L = plasma length
$\bar{L}_n$ = nozzle length
M = cold gas mass injected per pulse
$\dot{m}$ = total mass flow
$\bar{\dot{m}}$ = average mass flow
$m_{f,i}$ = maneuver point fuel mass, $i = 1, 2$
m_{PL} = payload mass
P = gas pressure
$\bar{P}$ = average laser power
$\hat{P}$ = defined in Eq. (12)
$\bar{P}_{DW}$ = detonation pressure rise
p = focal point length
Q = total laser energy absorbed
q = laser energy absorbed per unit mass
R = reflector system distance from Earth
r = polar radial coordinate
r_s = reflector mirror radius
r_0 = Earth radius
r_1 = low-Earth-orbit altitude
r_2 = geostationary-Earth-orbit altitude
t = time
t_{bi} = maneuver burning time or laser engine operating time, $i = 1, 2$
t_p = laser pulse duration
U = gas velocity
$\bar{U}_e$ = exit jet average velocity
V_D = detonation velocity
w = radial distance, Eq. (27)
w_i = percent of nozzle coverage by the laser beam
X = Cartesian horizontal coordinate
Y = Cartesian vertical coordinate
γ = specific heat coefficient ratio
ΔV = velocity increment
η = defined by Eq. (12)
η_h = engine efficiency
η_i = ionizing efficiency
θ_c = conical nozzle opening angle
λ = laser beam wavelength
ρ = gas density
τ_p = laser pulse period

Subscripts
B.T. = laser-supported detonation wave break through conditions
0 = upstream conditions
1 = downstream conditions

Superscript
* = chocked flow condition

Received Jan. 10, 1997; revision received Sept. 10, 1997; accepted for publication Sept. 16, 1997.

*Aerospace Engineer, M.Sc.; currently at Pratt and Whitney, United Technologies, P.O. Box 109600, M/S 710-14, West Palm Beach, FL 33410-9600.

†Associate Professor, Faculty of Aerospace Engineering.

I. Introduction

PROPELLING various kinds of objects in space requires careful consideration regarding the means to accomplish each different mission, such as launching a payload from Earth to orbit, orbital transfer, and changes in angle or trajectory

plane. For example, the required thrust level to launch a useful payload of 1000 kg from Earth to orbit by means of current chemical rocket propulsion is on the order of 10^5–10^6 N. For missions such as keeping trajectory parameters, necessitated by small perturbations caused by drag or Earth gravity, where a thrust level of no more than several newtons is needed, one might attempt to use one of the newer propulsion concepts such as electrical, nuclear, or, the newest, magnetoplasmadynamic.[1,2] These propulsion methods (except chemical propulsion) provide very high levels of specific impulse (1000–4000 s), but so far fail to achieve a substantial absolute thrust (typical 10^{-3} N).

The level of specific impulse determines the usable payload. The target is to optimize thrust and specific impulse for a selected mission. The concept of the laser propulsion system (LPS) is to use a laser beam as the energy source, thus accomplishing both high levels of thrust and specific impulse. Laser propulsion is classified today[3] as an interim region between chemical (conventional) and advanced (state-of-the-art) means of propulsion, achieving thrust in the range of 10^2–10^4 N and specific impulse of 800–3000 s. Among the different missions, orbital transfer is the most suitable for applying LPS because of the lack of alternative options that can provide high thrust and high specific impulse together. It is desired to provide a solution for the gradual increase in the need to transfer heavier payloads (such as communication satellites) from low Earth orbit (LEO) to geostationary Earth orbit (GEO), and vice versa, in a shorter time, while maintaining full control of the process from start to end. The thrust level required for such a mission is on the order of 10^4 N. It will be shown that LPS can provide such a level with more than 1000 s of specific impulse.

Although concepts exist such as flat-base detonation wave propulsion, double-pulse laser propulsion, and microwave propulsion, they are less likely to be applied for the mission of interest in this paper.[1–5] The characteristics of flat-base propulsion make it more likely to be employed for a ground-to-orbit launch mission.[1] Focusing on this specific mission, laser propulsion may be applied mainly by two methods:

1) Repetitively pulsed (RP)—high-power laser beam pulses fired at very high frequency into an engine nozzle onboard the space vehicle, through the nozzle exit cross section. The laser pulses ionize the working fluid (usually gas) inside the nozzle and ignite a plasma jet that expands through the nozzle to create a thrust pulse.

2) Continuous wave (CW)—a steady-state mode of operation. The laser beam is projected to the engine through an optical window located at the front of the engine. The gas absorbs the laser beam energy and expands through the nozzle to produce thrust. This is usually done with a nozzle similar to a converging–diverging chemical rocket nozzle.

Figure 1 illustrates these methods of operation, which are founded on the assumption that a high-power laser source exists, based either on a high mountain or on a space station.[4,5] The typical range of laser power is 0.5–1000 MW.[4] Both types apply low molecular gas (often hydrogen) that, in the plasma state, can easily reach temperatures as high as 10^4–10^5 K. Such values are necessary to create the high level of thrust required.

The main advantage of LPS is the decoupling of the energy source from the space vehicle. Other advantages are the simplicity and reliability of the propelling engine because of few moving parts, the lack of complicated plumbing, and the low fuel consumption as a result of the high specific impulse. The LPS based on the RP method is the simpler of the two. There is no need for an optical window (Fig. 1), and the design of the complete engine may be less heavy than in the CW system for the same mission. Nevertheless, improved performance may be achieved in the CW system because in the RP system thrust and specific impulse are formed as a series of pulses, whereas in the CW system thrust is constant in time and continuous. It may be added that in the RP system the plasma jet

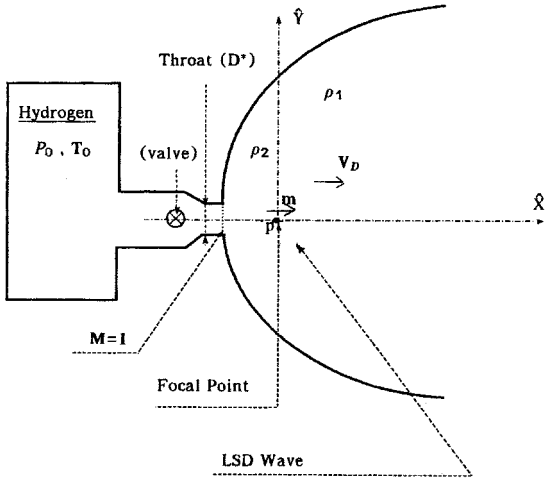

Fig. 1 Laser propulsion system modes of operation: a) continuous wave laser powered and b) repetitively pulsed laser powered.

is more stable, compared with a severe problem of plasma stabilization in the CW system.

Several LPS problems still need investigating, such as the method of pointing and focusing the laser beam into the nozzle exit, and the alignment between the thrust (nozzle) axis and the laser beam axis. The operational difficulties of LPS-based space vehicles, using a laser beam projected from Earth, may be overcome if a time window is defined. Consequently, a mission such as trajectory corrections for satellites may be performed during a defined limited time interval. One can calculate the location and timing for the laser firing to a predetermined point in space. A possible solution to the pointing and alignment problem is suggested in the Appendix. The solution applies to the orbital transfer mission discussed in this paper.

Further discussion will assume system operation in the RP mode, where the paper focuses on the operational mechanism and the design of a laser engine.

II. Physical Phenomena

The basic phenomenon that occurs inside the nozzle is the ionization of gas and plasma ignition. During the 1960s scientists succeeded in focusing a high-power laser beam to a rather small-diameter focal point (10^{-4} m) using mirrors and lenses.[6] With the laser engine, the parabolic nozzle is the means of achieving the same desired result.

When a laser beam is focused by the reflective parabolic nozzle at the focal point, its intensity is concentrated, and radiation intensities much higher than the threshold level for gas ionization and plasma formation may be achieved. The plasma is visible and referred to as a glow, also called a laser spark or light flash. The characteristic ionization threshold value for air at standard day (300 K, 10^5 Pa) is $I_{th} = 10^{15}$ W/m^2. As discussed in Ref. 6, such a value has already been achieved, using a 1-J laser source, with a pulse duration of 30 ns (laser peak power was 30 MW). The plasma residence time was 20–50 μs. As mentioned in the preceding text, the laser diameter at the focal point was about 10^{-4} m. It was also found that I_{th} reduces with pressure.

For gases such as hydrogen, Raizer[6] determined a characteristic range for the ionization threshold to be between 5×10^{14} and 1×10^{15} W/m^2. This is important to note because it is almost impossible to find a complete and final approach to determine I_{th}, according to Raizer.[6]

When plasma is ignited its length can be evaluated by using Eq. (1)

$$L = 2 \times V_D \times t_p \tag{1}$$

L (sometimes considered as width) is calculated by multiplying V_D and t_p. V_D (formed immediately when the plasma ignites, to be discussed later) is on the order of 10^5 m/s.[7] The pulse duration has an order of 10^{-8} s. That gives an initial plasma length on the order of only millimeters. L should be multiplied by two to represent plasma propagation in both directions.

When the laser pulse ends ionization of new cold gas in the vicinity of the initial plasma core still exists. This is because of the inverse bremsstrahlung (IB) effect described in the following text.

A. Inverse Bremsstrahlung Effect

The IB effect is the prime process assisting to achieve the very high plasma temperatures (10^4–10^5 K) necessary for laser engine operation and creation of high thrust. In the IB process free electrons are generated in the gas by the ionization process caused by the high-intensity laser beam. These free electrons are accelerated because they absorb the electromagnetic energy supplied by the laser beam. The major steps within the IB process are as follows.

1) Initial ionization takes place in the gas as a result of focusing the laser beam to high intensities (much higher than the threshold value), which generates free electrons. The initial L is in the range of 10^{-4}–10^{-5} m. At this plasma zone, the laser beam energy is absorbed in the gas. L is proportional to the electron mean free path in the gas. This ionization process is faster and, hence, shorter than a single laser pulse duration.

2) Free electrons are accelerated during the remainder of the laser pulse until its end. During that time the gas temperature rises, enhancing absorption of laser energy. L increases to 10^{-4}–10^{-1} m. This phenomenon is important because it is the cause of the expansion of the hot plasma region.

3) When the laser pulse terminates the high-speed electrons lose their energy because of random interaction with other particles in the gas. The high kinetic energy of the electron is converted into thermal energy, which, in turn, causes the nearby cold gas layer temperature to rise until it also reaches the plasma state.

The total energy absorbed in the gas during the IB process is

$$Q = K \times I \tag{2}$$

where Q is measured in units of W/m^3, I is in W/m^2, and K is in m^{-1}. K is the inverse of L

$$K = 1/L \tag{3}$$

High absorptivity of the gas is accompanied with higher L values, thus achieving lower K per Eq. (3), which, according to Eq. (2) defines a lower energetic deposition in the gas.

B. Laser Detonation

The plasma propagation mechanism in the engine nozzle is referred to as the laser detonation wave (LDW). This phenomenon occurs when the laser power is much higher than the required laser intensity ionization threshold value. When such conditions take place, the ionization degree is high enough to heat not only the core gas at the focal region, but also the cold gas layers near the focal region employing the IB effect. A propagation of the initial plasma region is then achieved toward the nozzle exit cross section in the form of a detonation wave. At first, the wave is supported by the laser pulse. After the laser pulse terminates, the detonation wave front exists because of the high energy absorbed in the plasma, causing further ionization of the cold gas layers. In 1964, Nelson, who is mentioned in Ref. 6, found that the majority of the laser energy is already absorbed in the plasma rather than in the gas, because the plasma ignited about 9 ns after firing the laser pulse, whereas its duration was 30 ns. Because L increases with temperature (and time), the location where the high-speed electrons come in contact with the cold gas front is eventually shifted away from the focal point. It should be noted that gas is discharged into the exhaust nozzle in a pulsating mode and its volume expands in time. The detonation front separates between the plasma and the colder gas. Consequently, L increases and the high-speed electrons can propagate to a longer distance. When the propagation distance of the plasma exceeds the outer boundaries of the cold gas cloud in the nozzle cavity, the electrons have nowhere to propagate to, and the detonation wave front simply evaporates into the vacuum outside the gas boundaries.

The properties of the specific impulse and the equivalent gas expansion velocity can be determined as a function of the detonation velocity:

$$q = QL/\rho_0 V_D \tag{4}$$

where ρ_0 is the initial gas density. Using Eqs. (2–4) we obtain

$$q = I_0/\rho_0 V_D \tag{5}$$

Then, assuming that the laser energy is fully converted into the kinetic energy of the plasma jet, the following may be written:

$$\tfrac{1}{2}\bar{U}_e^2 = q \tag{6}$$

From Eq. (6), it is easily derived that

$$\bar{U}_e = \sqrt{2q} \tag{7}$$

If one uses $I_{sp} = \bar{U}_e/g$, then

$$I_{sp} = (1/g)\sqrt{(2I_0/\rho_0 V_D)} \tag{8}$$

The expression for V_D can be evaluated by assuming a laser detonation wave moving at V_D through the gas. In the case of steady-state and one-dimensional conditions and in accordance with the Chapman-Jouguet (CJ) detonation theory,[8] the following set of conservation equations are used:

Mass:

$$\rho U = \rho_0 V_D \tag{9}$$

Momentum:

$$P + \rho U^2 = P_0 + \rho_0 V_D^2 \tag{10}$$

Energy:

$$e + (P/\rho) + \tfrac{1}{2}U^2 = e_0 + (P_0/\rho_0) + \tfrac{1}{2}V_D^2 + (I/\rho_0 V_D) \tag{11}$$

The index 0 indicates upstream conditions of the wave front. The factor $I/\rho_0 V_D$ represents the laser energy absorbed in the gas.

Two nondimensional parameters, $\hat{P}$ and η, are defined and incorporated in the following Hugoniot relation, which originated from the energy equation (11) and Eqs. (9) and (10):

$$\left[\frac{(\hat{P}-1)}{(1-\eta)}\right]^{1/2}\left[\frac{(1+\eta)(1-\hat{P})}{2} + (h-h_0)\frac{\rho_0}{P_0}\right] = \frac{I\rho_0^{0.5}}{P_0^{1.5}} \tag{12}$$

where $\hat{P} \hat{=} P/P_0$ and $\eta \hat{=} \rho_0/\rho$, and $h \hat{=} e + P/\rho$.

The Hugoniot relation represents a set of curves on the ($\hat{P}$, η) plane. Based on the CJ theory, the detonation velocity is

the velocity that satisfies the CJ conditions, i.e., Eqs. (9–11). When the laser energy is fully absorbed in the gas and the laser pulse had terminated, the CJ condition is achieved. According to Raizer[6] the theoretical detonation velocity is set to be

$$V_D = \left[\frac{2(\gamma^2 - 1)I}{\rho_0}\right]^{1/2} \tag{13}$$

III. System Structure and Operation

The main components of the LPS, whose schematics are illustrated in Ref. 2, are the high-power laser transmitter, the reflector, which directs the approaching laser beam from Earth to the space vehicle, and the space vehicle engine including its fuel tank. (Fuel tank is a reference for a reservoir of working fluid, e.g., a gas such as hydrogen. This is not the traditional fuel that requires an oxidizer as well.) The laser transmitter is supposed to be in the range of several hundreds of megawatts to be able to provide sufficient power to propel a useful payload from one orbit to another. A dedicated energy source should be assigned to provide the laser transmitter the needed power. The energy source would probably be an Earth power station or a solar-pumped laser mounted on a separate space station. The reflector is essentially a large mirror designed to direct the incoming laser beam from the laser source to the space vehicle. The size of the mirror depends on the laser wavelength as well as on the topographic location of the laser transmitter, e.g., on a high mountain. Because of the divergence of the laser beam, the diameter of the reflector depends on its distance from the laser source. The lower the mirror orbits in space, the smaller it could be. However, in low-orbiting-trajectories operation a coverage problem may emerge. This problem could be overcome by stationing several reflectors at different altitudes in space. The reflector dimensions can be stated as

$$r_s = 1.22(\lambda/D)R \tag{14}$$

For example, a 2.2-μm laser wavelength (most suitable for transmitting because of a minimum of atmospheric disturbances), a 5-m laser aperture diameter, and a GEO altitude of 36,000 km will result in about 19-m mirror radius.

The principal component of the space vehicle is the engine, which is designed to efficiently convert the laser beam energy into thrust. As mentioned in the preceding text, further discussion will assume operation in the RP mode. A powerful laser beam enters the engine nozzle through its exit cross section. Thus, the main components of the engine are the nozzle, the fuel tank, and a control system, combined with a suitable valve to regulate the gas flow rate injected into the nozzle.

The laser beam is focused to a focal region inside the nozzle, where an ionization process of the preinjected gas takes place. The ionized gas rapidly reaches the plasma state, and expands through the nozzle toward the exit cross section. Consequently, the nozzle has two main tasks: to focus the laser beam and to enable the proper expansion of the heated gas (plasma). The engine is in fact the nozzle itself, where ionizing and igniting the plasma as well as plasma expansion occur.

The nozzle is of a diverging (parabolic) type. The flow through the entire nozzle is supersonic. A conical contour of the nozzle can also be selected, where the cone half-angle is an optimization parameter for engine performance and beam-focusing efficiency. However, a much better design is to define a parabolic nozzle contour where all incoming parallel laser beams are reflected from the nozzle wall to the focal region of the parabola. Figure 2 is a schematic of a parabolic laser engine.

The laser energy loss from propagation in the atmosphere is described in detail in Ref. 9. For a finite nozzle length, the wall contour at its end is not parallel to the symmetric axis of the nozzle ($dr/dx \neq 0$). This could result in having a two-dimensional flow that may affect performance. The nozzle could be extended to end with a parallel section at the cost of extra weight. Typically, a parabolic contour such as

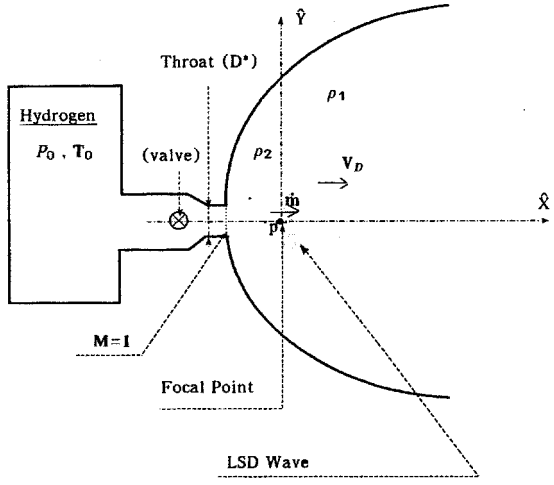

Fig. 2 Schematic of a laser engine.

$$Y^2 = 4pX \tag{15}$$

is selected for RP-operated LPS. This is also in accordance with the nozzle shape selected in chemical rockets.

The order of events occurring inside the engine operating in the RP method follows:

1) A powerful laser pulse is reflected by a reflector mirror into the engine nozzle.

2) The parabolic nozzle focuses the laser beam in its focal region. The theoretical focal point is defined by Eq. (15), representing the nozzle wall contour.

3) The focused and therefore intensified laser beam raises the temperature of the preinjected gas at the nozzle focal region, ionizes it, and initiates the plasma (the IB process).

4) The duration of the laser pulse is longer than the time required to create and ignite the plasma. Thus, immediately after plasma ignition, a laser detonation wave is formed that is supported by the energy of the remainder of the laser pulse. This phenomenon is referred as a laser-supported detonation wave (LSD). LSD occurs because the level of I achieved at the focal point is higher than the threshold intensity value required for the ionization. Absorption of laser energy continues all through the duration of the laser pulse. However, absorption is augmented by formation of the plasma, which has higher absorptivity to laser radiation.

5) The detonation wave progresses from the nozzle focal region toward its exit cross section, thus enabling the plasma to expand rapidly into the preinjected cold gas layer. The LSD formed, which is a spherical wave, starts to progress immediately after the plasma is formed. It continues also after the termination of the laser pulse, and only after the LSD has advanced to the boundaries of the preinjected gas.

6) While stages 3–5 take place, high pressure is created inside the nozzle, blocking the flow of new cold gas, stored in the fuel tank. At the end of the thrust cycle, when the pressure inside the nozzle drops, the gas flow restarts.

7) Thrust is produced from the pressure difference created through the nozzle wall, and exists as long as the detonation wave expands within the nozzle.

IV. Laser Engine System Dynamics and Properties

Thrust in the RP method is not constant in time and depends on the dynamic phenomena of the LSD wave. Thereafter, the pressure drops to the ambient values and thrust is reduced

drastically. The process starts when the cold gas is injected through a chocked valve (Fig. 2) into the nozzle from a gas reservoir. After a short period, during which the cold gas propagates toward the nozzle exit, the firing timing is set to allow the gas to pass the focal region. The gas is ionized, creating a hot plasma front (the LSD) propagating toward the exit plane of the nozzle. To optimize the thrust cycle it is best if the process terminates inside the nozzle. For convenience, we average parameters such as the thrust, laser power, and mass flow over τ_p:

$$\bar{F} = \frac{1}{\tau_P} \int_0^{\tau_p} F \times \mathrm{d}t \tag{16}$$

where $\bar{F}$ is obtained over τ_p. The mass average flow is

$$\bar{m} = M/\tau_P \tag{17}$$

$\bar{P}$ is

$$\bar{P} = E/\tau_p \tag{18}$$

Hence, the specific impulse will be

$$I_{\mathrm{sp}} = \bar{F}/g\bar{m} \tag{19}$$

According to Pirri and Simmons,[10] an equation estimating the specific impulse can be obtained

$$I_{\mathrm{sp}} = \frac{1}{g}\left(\frac{8E}{\pi\rho^* u^* D^* \tau_p}\right)^{1/2} \tag{20}$$

The variables ρ^*, u^*, and D^* are the properties of the cold gas that flows from the gas reservoir through the chocked valve into the nozzle.

P_{DW}, which is a characteristic of the LSD, is estimated as[2,6]

$$P_{DW} = \frac{\bar{\rho}_1(r) \times V_D^2}{1 + \gamma} \tag{21}$$

The density $\bar{\rho}_1(r)$ is the time-averaged gas density upstream of the LSD wave front. It is assumed (in accordance with Ref. 10) that a linear pressure distribution exists along the axis, reducing from a maximum value at the focal point to the temporal position of the LSD. The maximum pressure value reduces in time with the propagation of the LSD. This point is the meeting point between the LSD and the boundary of the preinjected cold gas and is named the breakthrough point (B.T.). The LSD vanishes exactly at B.T. and practically into the ambient vacuum. The pressure inside the nozzle is a function of time. At different times, the LSD is situated at a different nozzle position (and radius). The cycle-averaged thrust is

$$\bar{F} = \int_{r_0}^{r_{\mathrm{B.T.}}} P(r) \times \sin^2(\theta_c) \times 2\pi r \times \mathrm{d}r \tag{22}$$

$$P(r) = P_{DW}(r/r_{\mathrm{B.T.}}) \tag{23}$$

where r indicates the nozzle radius at the temporal LSD position, and r_0 and $r_{\mathrm{B.T}}$ are the focal radius and B.T. point radius, respectively. The angle θ_c is calculated for an equivalent conical nozzle that has walls tangent to the walls of the parabolic nozzle at its exit cross section.

V. Orbital Transfer Mission Application

The present study evaluates the feasibility of using a laser engine as a propulsion device suitable for a Hohmann orbital transfer (with a minimum energy requirement) of a small satellite, to be raised from LEO to GEO. Figure 3 illustrates that transfer. The relevant data are r_0 = 6378 km, r_1 = 300 km, r_2 = 36,000 km, space vehicle m_0 = 500 kg, and m_{PL} = 100 kg.

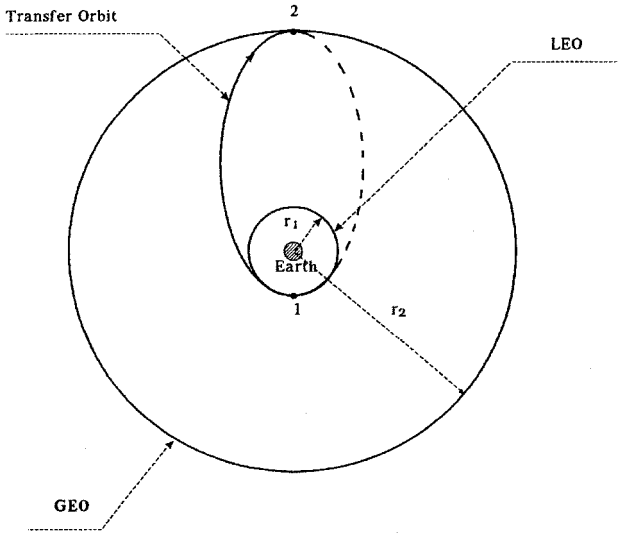

Fig. 3 Hohmann orbital transfer.

Velocity increments are applied when the space vehicle reaches 1) the perigee and 2) the apogee (Fig. 3). The velocities needed for such transfers are 2.42 km/s at point 1 and 1.46 km/s at point 2. The total trip time T from point 1 to point 2 is calculated as half of a full elliptical orbit, which gives the value of 19,115 s.

The laser engine is designed to operate at points 1 and 2 for a specified period of time. The time required for operating the laser engine is calculated, and indicates that it is on the order of typical burning time in conventional chemical rockets, and hence can be a suitable replacement. In general, the time for engine operation should be as short as possible, to support the main assumption that we are dealing essentially with thrust pulses at the two points. The short time also means a short distance covered by the space vehicle, compared with the orbital transfer distance and T. In addition, short periods are required to align the laser beam with the nozzle axis of symmetry.

The burning time at each point of the maneuver (operating time of the laser engine) is

$$t_{bi} = m_{f,i}/\dot{m} \tag{24}$$

where $m_{f,i}$ is at each point and $\dot{m}$ is from the nozzle. For each point, $m_{f,i}$ can be calculated by

$$\Delta V = I_{\mathrm{sp}} \times g \times \ell n(m_0/m_1) \tag{25}$$

where m_0 and m_1 are space vehicle masses before and after the maneuver.

The mass flow is

$$\dot{m} = \frac{2\eta_h \times \bar{P}}{(g \times I_{\mathrm{sp}})^2} \tag{26}$$

where η_h is defined by the ratio of kinetic energy of the plasma jet to $\bar{P}$ obtained at the focusing volume of the nozzle.[9] Typical (maximum) efficiency value predicted for the RP laser engine is 0.4.[9]

The selected values for the present mission are η_h = 0.36 (90% of maximum efficiency), I_{sp} = 1200 s, and $\bar{P}$ = 400 MW, which may be considered practical values. From these values we obtain $\dot{m}$ = 2.0782 kg/s, $\bar{F}$ = 24,464 N, t_{b1} = 44.7 s, t_{b1}/T

= 0.23%, t_{b2} = 22.9 s, and t_{b2}/T = 0.12%. These short periods of time justify the previous assumption of pulse operation.

VI. Nozzle Geometry and Laser Beam Focusing

The nozzle selected during the research was of a parabolic shape with a wall contour according to Eq. (15). Dimensions are L_n = 0.4 m, and parabolic nozzle p = 0.1 m.

The laser beam source distribution at the entrance to the nozzle is assumed to be of a Gaussian profile, typical for laser beams (Fig. 4):

$$I(r) = I_0 \exp(-2r^2/w^2) \tag{27}$$

Here, r is the radial distance from the axis of symmetry, and w is the radial distance at a specific cross section where the local intensity is reduced to e^{-2} of its local I_0 (the maximum value at the specific cross section).

A special ray-tracing computer program was developed to compute the I distribution at the focal region of the parabolic nozzle. Figure 5 illustrates a laser ray propagation in the nozzle.

Selecting the laser power (of 400 MW) and beam coverage to be 25% at the entrance cross section of the nozzle, we obtain a value for $I_0 = 2.5 \times 10^{10}$ W/m^2. Such calculations enable us to determine the I distribution at the focal region as well as the power loss at the nozzle.

To simulate an imperfect nozzle (a result of manufacturing difficulties of surface quality or deterioration), Eq. (15) was modified to include a surface contour perturbation. The perturbation simulates a surface roughness. Hence, the modified nozzle contour may be simulated as

$$Y = \sqrt{4pX} + A \times \sin[2\pi k(X/p)] \tag{28}$$

For practical values, k is selected to be 1000 (roughness cycle length is about 0.25 mm). The amplitude was varied between 0 (ideal nozzle) and 10 μm.

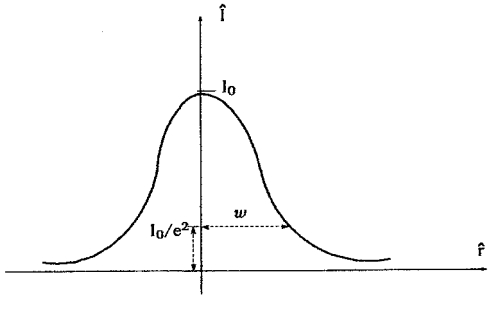

Fig. 4 Characteristic laser beam Gaussian intensity distribution.

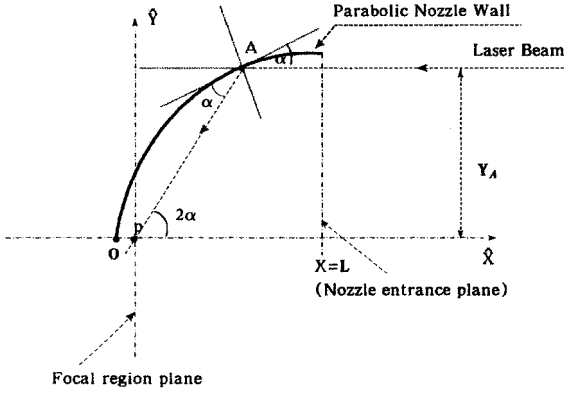

Fig. 5 Ray tracing.

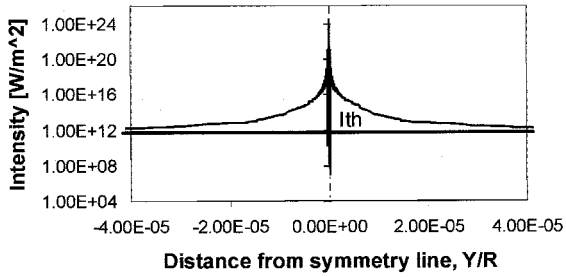

Fig. 6 Laser intensity distribution along the focal cross section for 25% laser coverage and zero roughness amplitude.

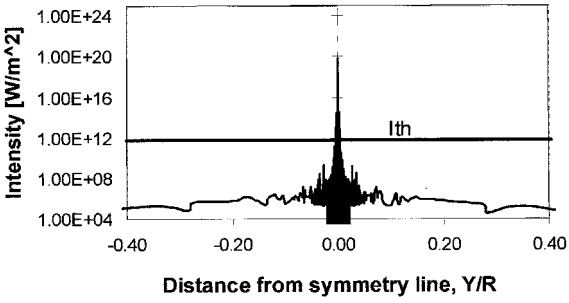

Fig. 7 Laser intensity distribution along the focal cross section for 25% laser coverage and 10^{-7} m roughness amplitude.

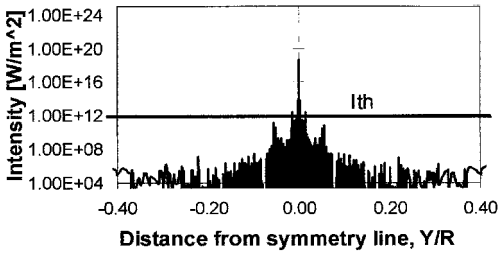

Fig. 8 Laser intensity distribution along the focal cross section for 25% laser coverage and 10^{-6} m roughness amplitude.

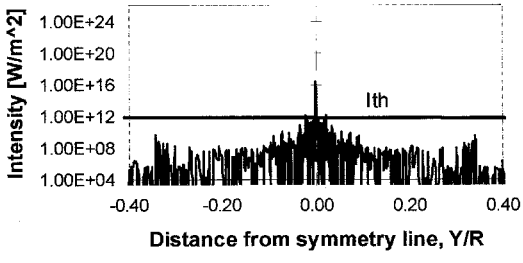

Fig. 9 Laser intensity distribution along the focal cross section for 25% laser coverage and 10^{-5} m roughness amplitude.

The relevant focusing characteristics of the nozzle may be determined by analyzing the percentage of laser power reflected into the focusing region. When we take into consideration the ionization threshold level of the specific fuel, we may define η_i as a measure of the amount (in percentage) of laser energy, which is focused within a region defined by a contour of radiation intensity that equals the ionization threshold level of the fuel.

Parametric study was performed with various amplitudes and several laser percents of nozzle coverages [$w_i = (w/R) \times 100$] at the nozzle entrance. The selected parameters were A_i: 0, 10^{-5}, 10^{-6}, 10^{-7} m, and i = 1–4; and w_i: 25, 50, 75, 100%, and i = 1–4.

The presented results (Figs. 6–10) were obtained in most cases with percentage of laser coverage at the nozzle entrance

Table 1 Laser power and loss resulting from ionizing efficiency at the focal region

Roughness amplitude, m								
10^{-5}		10^{-6}		10^{-7}		0		Laser coverage for fixed laser source, %
Loss, 100% η_i	Effective power, MW	Loss, 100% η_i	Effective power, MW	Loss, 100% η_i	Effective power, MW	Loss, 100% η_i	Effective power, MW	
71.1	110.2	20.8	310.9	1.6	386.5	0	392.7	25
95.6	33.8	75.0	192.3	27.3	559.5	0	769.7	35
97.7	35.8	76.9	362.6	45.8	851.0	0	1.57 GW	50

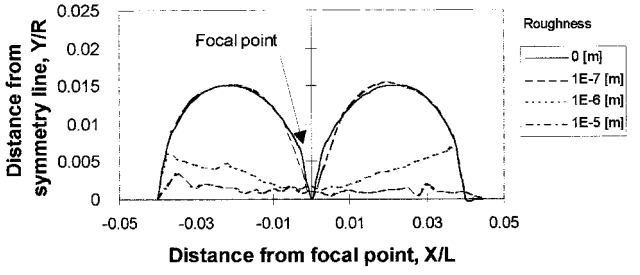

Fig. 10 Preliminary ionized region inside the nozzle for 25% laser coverage and various roughness amplitudes.

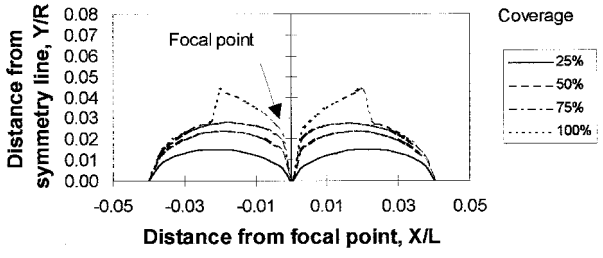

Fig. 11 Preliminary ionized region inside the nozzle for various laser coverages and zero roughness amplitude.

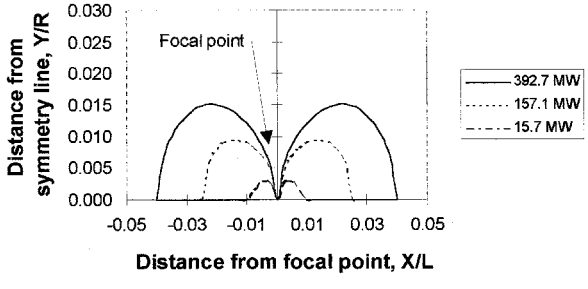

Fig. 12 Preliminary ionized region inside the nozzle for various laser power values (25% laser coverage, zero roughness amplitude).

of 25%. This value is within the optimal range of 20–35%.[11] In addition, the program was used to evaluate the preliminary ionized volume inside the nozzle as well as the ionization efficiency.

The required laser energy E_{req} per pulse at the nozzle entrance is

$$E_{\text{req}} = \bar{P}/(f \times \eta_i) \tag{29}$$

Calculation of E_{req} indicates a value of 50.5 kJ, with the laser operating at a frequency of 10^4 Hz. Assuming negligible atmospheric disturbances (based on proper selection of laser beam wavelength), these values may also represent the characteristics of the laser beam at its source.

VII. Results and Discussion

The laser intensity distribution inside the nozzle and the preliminary ionization volume and efficiency were calculated for the selected nozzle. Figures 7–9 illustrate the profile of the laser intensity distribution at the nozzle focal cross section for various roughness amplitudes. It is seen that the ionization threshold level has been surpassed only in a small and limited volume inside the nozzle. These profiles can be compared to a perfect nozzle surface, with zero roughness ($A_1 = 0$, Fig. 6). It is important to evaluate whether sufficient energy is focused in that region, hence enabling the desired levels of thrust and specific impulse for the selected mission. Even though the ionization threshold has been achieved in most conditions (albeit at different η_i), it is important to analyze the effect of roughness amplitude and laser coverage on the engine performance.

The contour of the location where the local intensity surpasses the threshold ionization value is shown in Fig. 10 for various roughness amplitudes and w_i of 25%. Figure 10 shows that the ionized volume shrinks with increases in roughness amplitude until there is practically no ionized volume for a roughness value of 10^{-5} m or higher. In Fig. 11, similar contours are given for various laser coverages and a zero roughness amplitude, which indicates a direct correlation between the laser coverage and the ionized volume. Figure 12 illustrates the effect of laser power on the preliminary ionized volume (zero roughness and 25% laser coverage), which increases monotonically with the laser power.

Table 1 summarizes computation of the total power and power loss caused by ionization efficiency for several combinations of laser coverage percentages and roughness amplitudes. It is seen that a roughness amplitude of 10^{-6} m or smaller should be selected for 25% laser coverage, and a 10^{-7} m value or smaller for 35% coverage. Another conclusion observed from Table 1 is that a 50% laser coverage cannot support the mission performance requirements because of the low ionizing efficiency (even with a high surface quality condition of 10^{-7} m).

Calculation of the engine performance, using a surface quality of 10^{-6} m, results in producing 19,600 N, which is 80.1% of the required thrust for the selected mission. This in turn can enable operation at the cost of 28% longer engine operation periods t_{b1}, t_{b2}. Such extended periods still justify the pulse operation assumption, as they both remain below 0.3% of total trip time.

Figures 13–15 illustrate the variation of required nozzle radius as a function of space vehicle mass, with a percentage of laser beam coverage as a parameter, for a fixed acceleration of $a = 5g$

$$a = \frac{\bar{F}}{m_0} = \frac{2\eta_i\eta_h\bar{P}}{m_0 \times gI_{\text{sp}}}\ \text{m/s}^2 \tag{30}$$

Here η_i evolved from Table 1 in accordance with wall A and laser coverage percentage.

Figures 14 and 15 describe the required nozzle characteristics, i.e., radius, percentage of laser coverage, and surface roughness amplitude, for a different mass of space vehicle. It is found that nozzle radius sensitivity (curve slope) is decreasing for higher laser coverage (50%). This fact enables an in-

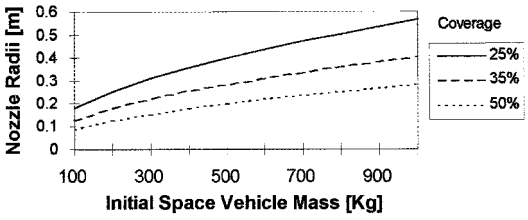

Fig. 13 Required nozzle radius vs space vehicle mass for various laser coverages (zero roughness).

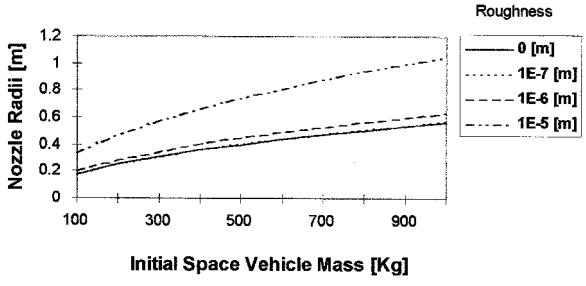

Fig. 14 Required nozzle radius vs space vehicle mass for various roughness amplitudes and 25% laser coverage.

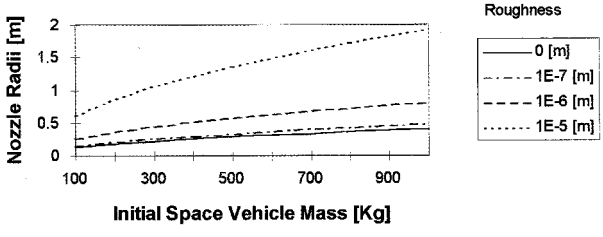

Fig. 15 Required nozzle radius vs space vehicle mass for various roughness amplitudes and 35% laser coverage.

crease in payload by a small increase in nozzle size. However, sensitivity to wall roughness amplitude, which is greater with an increase in percentage of laser coverage, still forces employment of a lesser coverage (25%) (Figs. 14 and 15). Using 25% coverage results in less penalty in engine performance with degradation in wall surface quality. For example, for a fixed nozzle radius of 200 mm, an increase in roughness from zero amplitude to 10^{-7} m (using 35% laser coverage) results in a payload reduction of about 100 kg. However, at 25% coverage the payload reduction as a result of similar wall surface degradation is an almost negligible amount. A further surface degradation to 10^{-6} m (at 25% coverage) still results in only a minimal payload reduction of about 20 kg.

VIII. Conclusions

This paper describes the RP laser propulsion mechanism and its feasibility for a specific mission. All major physical phenomena occurring inside the nozzle that contribute to thrust generation were taken into consideration.

For an orbital transfer mission raising a 500-kg satellite from 300-km altitude toward GEO orbit, a laser engine was found to be capable of producing 19,600 N of thrust with a specific impulse of 1200 s. Engine operation periods for the mission are 57 and 29 s in accordance with each step of the maneuver (less than 0.3% total trip time). These periods are on the order of chemical propulsion systems.

The nozzle selected has a parabolic shape that can be manufactured, for 25% laser beam coverage at the nozzle entrance, with a 10^{-6}-m surface roughness and still achieve the required performance. The typical η_i attributed to the LPS engine was found to be 79.2%. Laser coverage higher than 35% does not achieve system performance requirements (an impractical surface quality of 10^{-7} m is required). Results obtained in this work show that the laser source required for the described mission should have 30 ns t_p with energy per pulse of 50 kJ at a frequency of about 10^4 Hz.

We assume that such a powerful laser device will be available in the near future. Currently, one of the highest energy lasers, as described in the literature, is the GEKKO XII laser device, operating in Japan. It is capable of producing energy in the range of 25 kJ but at 1 ns only. Hence, significant improvements are still needed to comply with mission requirements, and further study on these devices is justified.

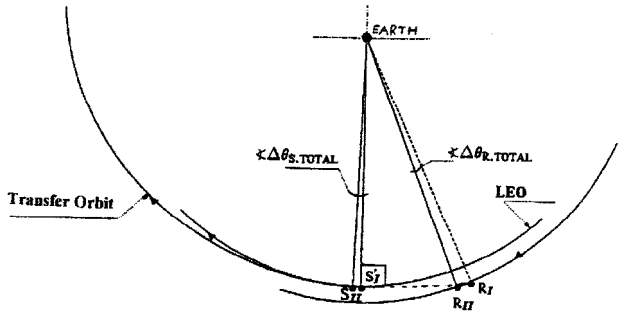

Fig. A1 Possible solution for the laser beam alignment problem.

Appendix: Laser Alignment

Figure A1 presents a scheme of a possible solution to the pointing and alignment problem. We assume the reflector mirror that directs the laser beam into the engine nozzle is in orbit 100 km above the orbiting space vehicle.

Point R_I represents the reflector location in respect to the space vehicle location in point S_I (point I is when the laser engine starts to operate at the beginning of the maneuver, i.e., the transfer orbit perigee). At that specific predetermined location, a laser beam projected from the reflector toward the engine nozzle will be fully aligned with the nozzle axis of symmetry. When the laser engine terminates its operation, both the reflector and the space vehicle will be at points R_{II} and S_{II}, respectively. Knowing t_{bi}, calculated in Eq. (24), and the orbital maneuver parameters at the LEO orbit point (also the perigee point), it is easy to evaluate the angle difference between the laser beam and the engine nozzle axis at point II (the angle difference is predetermined to be practically zero at point I). Calculations of these values show a relatively small change in alignment of no more than 0.5 deg, compared with the original full alignment between the reflector laser beam axis and the space vehicle nozzle axis (at point I). The ray-tracing computer program referred to in the preceding text was executed, taking as an input that same angle difference in alignment, up to 10 times as much, i.e., 5 deg. It was shown that the ionization threshold level was still achieved at those conditions, enabling the operation of the laser engine.

References

[1]Birkan, M. A. , "Laser Propulsion: Research Status and Needs," *Journal of Propulsion and Power*, Vol. 8, No. 2, 1992, pp. 354–360.

[2]Maxwell, C. D., and Myrabo, L. N., "Laser Driven Repetitively Pulsed MHD Generators—A Conceptual Study," *Orbit Raising and Maneuvering Propulsion: Research Status and Needs*, edited by Leonard H. Caveny, Vol. 89, Progress in Astronautics and Aeronautics, AIAA, New York, 1983, pp. 167–200.

[3]Kemp, N. H., and Rosen, D. I., "Laser Energy Absorption in Gases: Research Problems," *Orbit Raising and Maneuvering Propulsion: Research Status and Needs*, edited by Leonard H. Caveny, Vol. 89, Progress in Astronautics and Aeronautics, AIAA, New York, 1984, pp. 73–94.

[4]Rosen D. I., and Pirri, A. N., "Repetitively Pulsed Laser Propulsion: Needed Research," *Orbit Raising and Maneuvering Propulsion:*

Research Status and Needs, edited by Leonard H. Caveny, Vol. 89, Progress in Astronautics and Aeronautics, AIAA, New York, 1984, pp. 95–108.

[5]Bond, A., and Martin, A. R., "Concept Studies for a Laser Supported Orbital Transfer Vehicle," *Acta Astronautica Journal*, Vol. 19, No. 1, 1989, pp. 73–86.

[6]Raizer, Y. P., "Breakdown and Heating of Gases Under the Influence of a Laser Beam," *Soviet Physics Uspekhi*, Vol. 8, No. 5, 1966, pp. 650–673.

[7]McCay, T. D., "Experiments on Optical Discharges in Hydrogen," *Journal of Thermophysics and Heat Transfer*, Vol. 2, No. 4, 1988, pp. 317–323.

[8]Raizer, Y. P., "Heating of a Gas by a Powerful Light Pulse," *Soviet Physics JETP*, Vol. 21, No. 5, 1965, pp. 1009–1017.

[9]Hong, Z. C., and Chang, C. Y., "Laser Propulsion System Performance: Requirements for Single Stage to GEO Launch," International Astronautics Federation, IAF 94-s.3.421, Jerusalem, 1994.

[10]Pirri, A. N., and Simmons, G. A., "The Fluid Mechanics of Pulsed Laser Propulsion," *AIAA Journal*, Vol. 15, No. 6, 1977, pp. 835–842.

[11]Pirri, A. N., and Monsler, M. J., "Propulsion by Absorption of Laser Radiation," *AIAA Journal*, Vol. 12, No. 9, 1974, pp. 1254–1261.

[12]Kare J. T., "Laser Supported Detonation Waves and Pulsed Laser Propulsion," *Proceedings of the American Institute of Physics*, Vol. 208, 1990, pp. 359–364.

[13]Kemp, N. H., "Computer Simulation of Nonsteady Flow of a Real Gas with Laser Energy Absorption," AIAA Paper 84-1569, 1984.

[14]Kemp, N. H., and Legner, N. H., "Steady (CW) Laser Propulsion: Research Areas," *Orbit Raising and Manuvering Propulsion: Research Status and Needs*, edited by Leonard H. Caveny, Vol. 89, Progress in Astronautics and Aeronautics, AIAA, New York, June 1984, pp. 109–128.